
Clinical Impact of Respiratory Motion Correction in Simultaneous PET/MR with a Joint PET/MR Predictive Motion Model

Richard Manber¹, Kris Thielemans²,
Brian F Hutton^{2,3}, Simon Wan², Francesco Fraioli²,
Anna Barnes², Sébastien Ourselin⁴, Simon Arridge⁴,
and David Atkinson¹

¹Centre for Medical Imaging, Division of Medicine,
University College London, London, UK

²Institute of Nuclear Medicine, UCL and UCL
Hospitals, London, UK

³Centre for Medical Radiation Physics, University of
Wollongong, New South Wales, Australia

⁴Centre for Medical Imaging Computing, Faculty of
Engineering, University College London, London, UK

04/12/2017

Richard Manber: Institute of Nuclear Medicine, 5th floor, Tower, University College Hospital, 235 Euston Road, London, NW1 2BU. Tel.: +4420 3447 0535, E-mail: manber.richard@gmail.com
Funding: Siemens/UCL IMPACT studentship, EPSRC (EP/K005278/1) and NIHR University College London Biomedical Research Centre.

Word count: 5465 Running title: Impact of PET/MR Motion Correction

ABSTRACT

In Positron Emission Tomography (PET) imaging, patient motion due to respiration can lead to artefacts and blurring, in addition to quantification errors. The integration of PET imaging with Magnetic Resonance (MR) imaging in PET/MR scanners provides spatially aligned complementary clinical information, and allows the use of high spatial resolution and high contrast MR images to monitor and correct motion-corrupted PET data. We test our PET respiratory motion correction methodology based on a joint PET-MR motion model, on a patient cohort, showing it can improve lesion detectability and quantitation, and reduce image artefacts.

Methods: We apply our motion correction methodology on 42 clinical PET-MR patient datasets, using multiple tracers and multiple organ locations, containing 162 PET-avid lesions. Quantitative changes are calculated using Standardised Uptake Value (SUV) changes in avid lesions. Lesion detectability changes are explored with a study where two radiologists identify lesions, providing confidence levels, in uncorrected and motion-corrected images.

Results: Mean increases of 12.4% for SUV_{peak} and 17.6% for SUV_{max} following motion correction were found. In the detectability study, an increase in confidence scores for detecting avid lesions is shown, with a mean score of 2.67 rising to 3.01 (out of 4) after motion correction, and a detection rate of 74% rising to 84%. Of 162 confirmed lesions, 49 lesions showed an increase in all three metrics SUV_{peak} , SUV_{max} and combined reader confidence scores, whilst only two lesions showed a decrease. We also present clinical case studies, demonstrating the effect respiratory motion correction of PET data can have on patient management, with increased numbers of lesions detected, improved lesion sharpness and localisation, as well as reduced attenuation-based artefacts.

Conclusion: We demonstrate significant improvements in quantification and detection of PET-avid lesions, with specific case study examples showing where motion correction has the potential to have an effect on patient diagnosis or care.

Keywords Motion Correction · PET/MR · Lesion Detection · Lesion Quantification

INTRODUCTION

Due to long acquisition duration (typically 3-15 minutes per bed position), motion during PET acquisition may lead to blurring in resulting images and errors in quantification (1,2). The already limited spatial resolution of PET, around 4.5 mm full width half maximum, is effectively reduced when motion occurs during acquisition. In oncology, tumours in the upper abdomen and thorax are particularly adversely affected by respiratory motion, due to a movement of the diaphragm of around 20 mm on average in one breathing cycle (3). Lesions at anatomy boundaries such as between the liver and lung can also be mispositioned on images when compared to the anatomical reference MR or CT image. Furthermore, quantification is affected as moving lesions show an apparent increase in size and decrease in uptake as the lesion appears smeared. Motion may also cause problems with attenuation correction, where a static attenuation map does not correlate spatially with the PET emission data, due to moving anatomy (4).

PET respiratory motion correction can be achieved by gating (splitting data into respiratory states), reconstructing separate images and registering to a common respiratory state (2,5,6). This technique requires a good signal-to-noise ratio in each gated image for accurate registration results. This becomes difficult with pressures of reducing scan time and lowering patient dose, leading to low count statistics and lower signal-to-noise ratio in each gate. The recent advent of PET/MR scanners allows exploitation of modality simultaneity by using high spatial resolution and high contrast MR images to estimate respiratory motion and correct PET data, without additional radiation exposure, with MR tagging (7,8), or by acquiring quick 'motion-capturing' 2D images (9) or low resolution 3D images (10).

Although current methods for respiratory motion correction in PET/MR show an improvement in PET image quality, all require a change to the otherwise intended PET/MR protocol to be able to collect the respiratory signal and/or MR-derived motion model in a clinical setting. Many methods use external monitoring device to obtain a respiratory signal, which requires time for set-up and readjustment, and can fail due to mispositioning, patient movement, poor calibration, or signal drift and clipping. Some methods also require alteration to MR sequences which need to be set up in advance

of the scan, can create artefacts in MR images near the diaphragm, and may increase scan time.

In recent work, we demonstrated the capability of a joint PET-MR respiratory motion model built using data from a 1 minute dynamic MR sequence, and with no external hardware required (11). The methodology addressed many of the limitations found with the discrete binning method used in our previous work (12). In this current work, we perform a pilot analysis to test the methodology on a larger patient cohort, by examining change in SUV metrics on attenuation corrected PET reconstructions and by performing a lesion detectability study. In this study, two readers examine each uncorrected and motion-corrected image and mark suspected lesions with a confidence score, so the true-positive (TP) and false-positive (FP) detection rate can be calculated, as well as changes in confidence scores between uncorrected and motion-corrected images. Finally, we present a number of illustrative examples, to demonstrate how respiratory motion correction may have the potential to affect clinical patient management, for example, on patient staging, diagnosis and surgical planning.

MATERIALS AND METHODS

Respiratory Motion Correction via Joint PET-MR Motion Model

In our recent work, a methodology for a joint PET-MR motion model was described, using one minute of simultaneously acquired PET and MR data to provide a respiratory motion model that captured inter-cycle and intra-cycle breathing variations (11). The continuous nature of the model allows interpolation and extrapolation at any respiratory signal value, meaning 100% of PET data is used in the reconstruction, and deformation fields are estimated even at extreme values such as at deep inhale for the MRAC sequence. All slices of the free-breathing MR acquisition are used, with an optimisation scheme to form the model that is robust to registration errors at single slices. MR and PET data were also aligned temporally by including a time-shift in the optimisation while taking the different hardware clock-rates into account. The motion model links one or more surrogate measures of respiratory motion to the tissue deformation. In our previous work, we found the best

performance was achieved when using the PET-derived respiratory signal and its gradient in a 2-surrogate model. The model used a linear fit to relate the surrogates to the deformations. This scheme is used in the current work, on a larger patient data set, to estimate deformations throughout the PET scans.

Study Design

The UK Health Research Agency approved this retrospective study and the requirement to obtain informed consent was waived. All data were acquired using an integrated 3T PET/MR system (Biograph mMR, Siemens Healthcare).

Data were retrospectively analysed from 42 patients whom had undertaken PET/MR scans between February 2014 and November 2015, selected based on clinical information suggesting possible avid regions in the thorax or abdomen. Tracers used were ^{18}F -FDG (24 patients) and ^{68}Ga -DOTATATE (18 patients). The patient cohort consisted of 18 women and 24 men, with a mean patient age of 61.9 years (range, 36-85 years).

The PET/MR imaging protocols included an additional breath-hold Dixon scan and a one minute free-breathing dynamic MR sequence (2D multi-slice gradient echo (1 min), sagittal slices at 9 slice locations, covering the thorax and abdomen (including lungs, liver, pancreas etc.) repeated 60 times. Scan parameters: slice thickness 10mm, gap between slice centres 25 mm, repetition time 5.1 ms, echo time 2.5 ms, flip angle 10° , pixel bandwidth 965 Hz, matrix size 192 x 144, FOV 262 x 349 mm, in-plane resolution $1.8 \times 1.8 \text{ mm}^2$, IPAT 3, acquisition time per image 0.3 s), used for quality monitoring related to breathing and MRAC. Data from the one minute MR sequence was used here to build the patient-specific motion model. Four consecutive minutes of PET list-mode data were used for the PET reconstructions presented here, with the mean time interval from radiotracer injection to this PET data being acquired being 1 hour 39 minutes \pm 33 minutes. The four minutes of PET data used here include the one minute of cine MRI acquisition and the preceding three minutes

Data Processing

A motion-compensated reconstruction of four minutes from the PET acquisition was carried out using deformation fields estimated by the 2-surrogate linear model, with PET data gated before reconstruction using the patient-specific scheme outlined in (11). For motion-corrected reconstructions, the attenuation μ -map was warped to each gate with deformation fields estimated by the motion model, using the values of the surrogate signal during the MRAC sequence acquisition. For uncorrected reconstructions, the acquired static μ -map was used. An ordered-subset expectation maximization reconstruction algorithm was used, with 21 subsets, 3 iterations, and 4-mm gaussian post-filtering, with randoms and scatter correction.

PET data processing (unlisting, reconstruction etc.) was carried out with STIR (Software for Tomographic Image Reconstruction) (13). All other analysis was performed with Matlab (Mathworks, Inc.) and MIRT (Medical Image Registration Toolbox) (14) was used in Matlab for registration.

Analysis

Lesion Detectability Study

The effect of motion correction on lesion detectability and localisation was assessed with a lesion detection study. Two accredited radiologists viewed the uncorrected and motion-corrected PET images for each patient data set on their own, without the benefit of any structural MR images. The viewing was done individually, and blinded. Images were read in two sets, with the uncorrected and motion-corrected images for each patient split between the two sets randomly, and with at least a two week interval between reads of each set to minimise recall bias. Each reader was free to scroll through slices and adjust colour scales. The readers were instructed to detect the presence of focal areas of tracer uptake higher than background activity, and which had the potential to represent pathological change and influence clinical decision. They were asked to mark suspected lesions on each image, with a four-point confidence score χ . This was defined as the presence of a lesion at each location being either:

- $\chi=1$. questionable (<50% likely)

- $\chi=2$. possible (50-75% likely)
- $\chi=3$. probable (75-95% likely)
- $\chi=4$. definite (>95% likely)

Scores provided by reader 1 and reader 2 are referred to as χ_1 and χ_2 respectively. The perceived anatomical locations of the lesions on the uncorrected and motion-corrected PET images were also documented with each mark by each reader.

For the purpose of this study, the reference standard used to define the presence and locations of lesions was a consensus read by the radiologists, using combined reading of all imaging studies, including original uncorrected PET, MR component of the hybrid PET/MR study, contemporaneous formal MR and CT and all follow-up imaging (CT, MR, PET), where available. Lesions marked by the two readers in uncorrected and motion-corrected images were matched visually to the reference read. Each marked lesion that matched a lesion in the reference was defined as a true-positive (TP), and any lesion in the reference that was not marked by the reader was defined as a false-negative (FN) and given a score of 0. Each marked lesion that did not match a lesion in the reference was defined as a false-positive (FP).

For all lesions in both the TP and FP sets, change in confidence rating for each lesion, $\Delta\chi$ is defined as the χ score for the motion-corrected image minus the χ score for the uncorrected image. For readers 1 and 2 these are referred to as $\Delta\chi_1$ and $\Delta\chi_2$ respectively. An increase in these values represents an increase in detection confidence, and a decrease represents a decrease in detection confidence after motion correction.

SUV Analysis

Change in two SUV metrics for lesions were assessed; $\Delta\text{SUV}_{\text{peak}}$, defined as the maximum average activity concentration within a 12 mm diameter sphere inside a manually defined region of interest (15), and $\Delta\text{SUV}_{\text{max}}$, defined as the maximum voxel SUV value inside the region of interest.

Statistical Analysis

Significance of differences in lesion detection confidence scores between uncorrected and motion-corrected images was made with the Wilcoxon signed rank test. For SUV metrics of lesions a paired sample t-test test was used.

RESULTS

In total, there were 162 PET-positive lesions (74 ^{68}Ga -DOTATATE, 88 ^{18}F -FDG) in the patient data (identified in the radiologist reference read), in the form of liver, pancreas, kidney, bowel, rib and shoulder lesions, as well as an assortment of nodes and areas of benign uptake, spread across 32 patients. We use the term 'lesion' to describe any of these marked areas of focal tracer uptake. 10 patients had no identifiable or lesions. We use the term 'lesion' to describe any of these marked areas of focal tracer uptake. These are summarised in Table 1.

Of 162 reference lesions, 72 were also confirmed to be present on MR, seven on CT, and 62 on both MR and CT. 21 lesions were confirmed either from PET follow-up, or from PET only considering patient history and information. A quantitative analysis summary is provided in Table 2.

Lesion Detectability

The TP rate, or sensitivity, for uncorrected and motion-corrected images was 85% and 95% respectively for reader 1, and 62% and 73% respectively for reader 2. On average, between the two readers over all 162 lesions, the TP rate was 74% (79% Ga only, 69% ^{18}F -FDG only) in the uncorrected images, rising to 84% (89% ^{68}Ga -DOTATATE only, 80% ^{18}F -FDG only) in the motion-corrected images.

Fig.1 shows $\Delta\chi$ scores for TP results, with positive change showing an increase in lesion detectability. Figure 1A shows $\Delta\chi$ distribution for all 162 lesions, for each reader separately. Considering the average of $\Delta\chi_1$ and $\Delta\chi_2$ over all 162 lesions, 8% (13 lesions) showed a decrease, 69% (112 lesions) showed no change, and 23% (37 lesions) showed an increase in confidence ratings. Between the two readers, there was a significant increase in mean detection confidence score for TP results, from 2.67 (2.92 ^{68}Ga -DOTATATE, 2.46 ^{18}F -FDG) in the uncorrected images, to 3.01 (3.21 ^{68}Ga -DOTATATE, 2.85 ^{18}F -FDG) in the motion-corrected images ($p < 0.0001$).

Fig. 1C shows the sum of detection scores $\Delta\chi_{1+2}$ for each lesion. Overall, 11% (18 lesions) showed a decrease (range -4:-1), 53% (86 lesions) showed no change, and 36% (58 lesions) showed an increase (range +1:+8).

There was a significant increase in summed detection confidence scores, $\Delta\chi_{1+2}$ from the uncorrected images to the motion-corrected images, for all TP lesions ($p < 0.0001$).

We aimed to reduce the intrinsic intra- and inter-observer variability of the scoring test by examining score changes where $\Delta\chi_1$ and $\Delta\chi_2$ are either both positive or both negative; where the two readers are in agreement as to whether a lesion has increased or decreased in detectability. There were 14 lesions where this was the case, with one lesion showing negative change for both readers (range -1:-2), and 13 lesions showing positive change for both readers (range +1:+4). For four of these lesions, confidence scores changed from 0 in the uncorrected images for both readers, i.e. lesions which were invisible to both readers in uncorrected images, then detectable to some degree in the motion-corrected images to both readers.

The total number of FP detections, combining results from both readers, was 30 (7 ^{68}Ga -DOTATATE, 23 ^{18}F -FDG) in uncorrected images and 21 (8 ^{68}Ga -DOTATATE, 13 ^{18}F -FDG) in motion-corrected images. Overall, 27 lesions showed a decrease, three lesions showed no change, and 16 lesions showed an increase in confidence ratings, for marked areas assumed to not be true lesions from the reference read.

SUV Analysis

Over all 162 reference lesions, there was a significant increase in both SUV_{peak} ($p < 0.0001$) and SUV_{max} ($p < 0.002$), with a mean increase in SUV_{peak} of 12.4% (12.6% ^{68}Ga -DOTATATE, 12.2% ^{18}F -FDG), and a mean increase in SUV_{max} of 17.6% (17.2% ^{68}Ga -DOTATATE, 17.9% ^{18}F -FDG), via motion-correction.

Fig. 2 shows $\Delta\text{SUV}_{\text{peak}}$ and $\Delta\text{SUV}_{\text{max}}$ for all lesions. Of all lesions, 14% (22 lesions) showed a decrease, and 86% (140 lesions) showed an increase in SUV_{peak} , whilst 17% (27 lesions) showed a decrease, and 83% (135 lesions) showed an increase in SUV_{max} .

Defining 'considerable change' as only those with a magnitude of change greater than 5% for both $\Delta\text{SUV}_{\text{peak}}$ and $\Delta\text{SUV}_{\text{max}}$; 3% (five lesions) showed considerable decrease, 43% (69 lesions) showed inconsiderable change, and 54% (88 lesions) showed considerable increase. The five lesions that showed considerable decrease were a lung node, lung lesion, rib lesion and two bowel lesions.

Cross-study Correlation

Overall, considering the three metrics of $\Delta\text{SUV}_{\text{peak}}$, $\Delta\text{SUV}_{\text{max}}$, and $\Delta\chi_{1+2}$ for the 162 reference lesions, two lesions showed a decrease in all metrics and 49 showed an increase in all metrics. Those that showed negative change were a mediastinal lymph node and a bowel lesion.

Clinical Case Studies

We present a number of case study examples to show the effects of motion correction on PET images, considering potential to affect clinical patient management. Clinical MR images presented were either acquired at exhale breath-hold or triggered, with data only collected at the exhale position. Uncorrected and motion-corrected images are displayed with the same colour scale for each case study.

Case Study 1: New Lesions Detected with MR confirmation

Case study 1 is a ^{68}Ga -DOTATATE scan of a patient (age 70-80) whom had recurrent neuroendocrine liver metastases post partial hepatectomy. A contemporaneous MRI showed at least two suspicious lesions in the remnant liver and several smaller concerning deposits.

In total, change in detection scores for three very small lesions was $\Delta\chi_{1+2} = [+1,+1,+1]$, with six of the total reads (3 lesions \times 2 readers) providing three newly detected lesions in the motion-corrected images. All three were found to be present in the MR images during the consensus reference read. Fig. 3A shows one of the newly detected lesions in uncorrected and motion-corrected images, with the lesion contrast appearing much greater in the motion-corrected image. SUV results verify these results, with increases in SUV metrics for the three lesions (Fig. 3B).

At least three lesions demonstrate DOTATATE avidity, suggesting metastatic neuroendocrine lesions. This information would influence decision regarding choice of treatment, which may be drug treatment (e.g. octreotide analogue), percutaneous ablation or resection.

Case Study 2: New Lesions Detected with PET Follow-up confirmation

Case study 2 is a ^{68}Ga -DOTATATE scan of a patient (age 40-50) known to have multiple endocrine neoplasia syndrome type 1 and known pancreatic lesions. A PET/MR scan was requested to assess lesion uptake and determine possible surgical approach.

Although the lesions were not verified in the MR images available, six lesions were confirmed as present in the reference read due to visibility in a follow-up scan carried out one year later (Fig. 4).

The increased number of detected lesions in the baseline scan is crucial. Accurate mapping of the number and location of tumours in the pancreas is critical for the evaluation of the risk vs benefit balance of surgical intervention, and to plan for the operation if surgery is pursued. The larger the extent of pancreatectomy, the more complex the surgery would be and the risk of subsequent diabetes as a complication.

Case Study 3: Lesion Localisation Change

Case study 3 is an ^{18}F -FDG scan for a patient (age 40-50) with known liver metastases found in a previously acquired CT scan.

Lesion localisation for one reader changed from lung to liver following motion correction. The reference read for this patient showed eight lesions, with all confirmed in the liver on the MR. This change in location is demonstrated in Fig. 5A, showing a PET maximum intensity projection of the uncorrected image. The location of the two lesions at the lung/liver interface is unclear in both the non-attenuation corrected and attenuation corrected images, however in the motion-corrected image, it is clear that the lesions are located in the liver. The fused PET/MR images show better spatial alignment of the PET and MR images in the motion-corrected case in Fig. 5B.

This large change in location is due to the MRAC being inadvertently acquired at deep exhale, and this is being corrected for in the method. The alignment of the MRAC meant large changes in $\Delta\text{SUV}_{\text{peak}}$ (+142% and +366%), for the lesions which appeared to move from the lung in the uncorrected image to the liver in the motion-corrected image.

The correction of lesion localisation through motion correction is important for staging and treatment planning. Involvement of more organs by metastases could

potentially changes disease stage, influence treatment decisions and infer a different prognosis.

Case Study 4: Intra-Lesion Activity Distribution Change

Case study 4 is a ^{68}Ga -DOTATATE scan (age 60-70). In this patient, detectability confidence scores showed either no change or a slight increase in all 11 lesions identified in the reference read. The shape of the activity distribution in three of these lesions was changed due to motion correction (Fig. 6). These are necrotic lesions with uptake on the outer edge of the lesion.

Although lesion detection and localisation has not been significantly changed, the uptake distribution within lesions could be of clinical importance. For example, change in intra-lesional uptake distribution may influence the perceived optimal site for PET directed biopsy in some patients, or in PET guided radiotherapy modulation in others.

Case Study 5: Artefact Reduction

Case study 5 is a ^{68}Ga -DOTATATE scan (age 50-60). The artefact in the uncorrected image due to a mis-aligned attenuation map has been corrected in the motion-corrected image (Fig. 7). In the PET images it is clear that the banana artefact at the top of the liver has been removed and the shape of high uptake in the stomach has been restored to match the shape of the stomach as seen in the MR. The motion-corrected PET image now spatially aligns better with the MR.

DISCUSSION

This work has provided a pilot analysis for a clinical validation of our joint PET-MR model-based motion correction method. Significant increases in all tested metrics have been shown in reference lesions, with mean increases of 12.4% and 17.6% in SUV_{peak} and SUV_{max} respectively, in 162 PET-avid lesions. We also showed an increase in confidence scores of readers detecting avid lesions, with a mean score of 2.67 rising to 3.01 through motion correction, and a TP rate of 74% rising to 84%. We found only two lesions that showed a decrease in all three metrics SUV_{peak} , SUV_{max} and $\Delta\chi_{1+2}$, whilst 49 lesions showed an increase in all metrics.

A number of clinical examples were presented to understand the range of positive effects that respiratory motion with our methodology correction can have, including newly detected lesions, increased lesion sharpness and detectability, artefact reduction, and better lesion localisation and intra-lesion activity distribution.

In the SUV analysis, (Fig. 2), the apparent outliers arise from good results, where the large increases in lesion SUV_{peak} and SUV_{max} are due to attenuation map misalignment being corrected through motion correction. The only five lesions that show considerable (more than 5%) decrease in SUV measurements could be due to the lesion locations. Two of these (including the largest decrease of 25%) were lesions located in the bowel, which is an area in which the motion model cannot predict motion due to bowel motion being sporadic and unrelated to respiration. Another was located on a rib, which could have suffered from poor deformation estimation due to the lack of sliding motion in the registration scheme, and the other two were in the lung of one patient with a very large lung mass, potentially causing unpredictable breathing patterns.

For the lesion detectability study, when considering combined lesion confidence scores from both readers, 11% of lesions showed a decrease and 36% showed an increase in detectability, with a much smaller range in the decrease set (-4:-1 vs. +1:+8).

One limitation of the detectability study was intra- and inter- observer variability in interpretation of imaging studies. The inter-reader variability observed here was higher than might be expected for a PET study focussing on a specific clinical context. However, the current study used multiple cohorts of patients and diseases. In addition, the PET images were initially read in isolation to assess detectability, without clinical patient information or structural images from MR/CT.. We attempted to overcome this by analysing results from both readers together. For example, when looking at only results where $\Delta\chi$ was either positive or negative for both readers in all reference lesions, 13 lesions showed an increase in detectability and only one showed a decrease. However, this single lesion had a higher SUV_{peak} and SUV_{max} in the motion-corrected image than the uncorrected image, suggesting that the negative $\Delta\chi$ was also due to human error.

A recommended approach to test lesion detectability is Free-response Receiver Operating Characteristic analysis (16). We did not carry out this analysis due to a

lack of a consistent reference standard and no definite method to identify false-positives. In the literature, PET-based detection studies revolving around testing different reconstruction methods (17), different acquisition times (18), motion correction (19), or time-of-flight impact (20), use phantom or simulated PET data, where a ground truth is known. The information that PET provides is unique in that it is portraying tracer uptake, unique to the modality. For example a lesion may appear avid in a PET image but this does not mean it will necessarily be visible in an MR or CT image.

The lack of a definite way to define false-positives (a PET avid lesion may not appear in MR or CT) applies to the results presented in this work for the FP rate, where 30 lesions were detected in the uncorrected images and 21 in the motion-corrected images, from 84 data sets (42 patients \times 2 readers). These are marked as false-positives due to the lack of evidence in the patient information or other modality, but in reality some of these may be real lesions.

We consider the work in this a pilot analysis. With streamlined pipeline and enhanced data processing efficiency, this can be adopted into routine practice, which in turn would provide the substrate needed for wider clinical validation.

CONCLUSION

We have demonstrated significant improvements in quantification and detection of PET-avid lesions in multiple tracers and multiple organ locations, with specific case study examples showing where motion-correction has the potential to have an effect on patient diagnosis or care.

ACKNOWLEDGEMENTS

We acknowledge support from: Siemens/UCL IMPACT studentship, the EPSRC (EP/K005278/1) and support by The National Institute for Health Research University College London Hospitals Biomedical Research Centre. In addition, thanks to David Brown and Robert Shortman at UCLH.

REFERENCES

1. Nehmeh SA, Erdi YE. Respiratory motion in positron emission tomography/computed tomography: a review. *Semin Nucl Med.* 2008;38:167-176.
2. Bai W, Brady M. Motion correction and attenuation correction for respiratory gated PET images. *IEEE Trans Med Imaging.* 2011;30:351-365.
3. Martinez-Möller A, Zikic D, Botnar RM, et al. Dual cardiac-respiratory gated PET: Implementation and results from a feasibility study. *Eur J Nucl Med Mol Imaging.* 2007;34:1447-1454.
4. Sureshbabu W, Mawlawi O. PET/CT Imaging Artifacts. *J Nucl Med Technol.* 2005;33:56-161.
5. Klein G, Reutter B, Huesman R. Non-rigid summing of gated PET via optical flow. *IEEE Nucl Sci Symp Conf Rec.* 1996;1339-1342.
6. Boucher L, Rodrigue S, Lecomte R, Bénard F. Respiratory gating for 3-dimensional PET of the thorax: feasibility and initial results. *J Nucl Med.* 2004;45:214-219.
7. Guérin B, Cho S, Chun SY, Zhu X, Alpert NM, El Fakhri G, et al. Nonrigid PET motion compensation in the lower abdomen using simultaneous tagged-MRI and PET imaging. *Med Phys.* 2011;38:3025-3038.
8. Chun SY, Reese TG, Ouyang J, et al. MRI-based non-rigid motion correction in simultaneous PET/MRI. *J Nucl Med.* 2012;53:1284-1291.
9. Würslin C, Schmidt H, Martirosian P, Brendle C, Boss A, Schwenzer NF, et al. Respiratory motion correction in oncologic PET using T1-weighted MR imaging on a simultaneous whole-body PET/MR system. *J Nucl Med.* 2013;54:464-471.
10. King AP, Buerger C, Tsoumpas C, Marsden PK, Schaeffter T. Thoracic respiratory motion estimation from MRI using a statistical model and a 2-D image navigator. *Med Image Anal.* 2012;16:252-264.
11. Manber R, Thielemans K, Hutton B, et al. Joint PET-MR respiratory motion models for clinical PET motion correction. *Phys Med Biol.* 2016;17:6515-6530.
12. Manber R, Thielemans K, Hutton BF, et al. Practical PET respiratory motion correction in clinical PET/MR. *J Nucl Med.* 2015;56:890-896.
13. Thielemans K, Tsoumpas C, Mustafovic S, et al. STIR: software for tomographic image reconstruction release 2. *Phys Med Biol.* 2012;57:867-883.

-
14. Myronenko A, Song X. Intensity-based image registration by minimizing residual complexity. *IEEE Trans Med Imaging*. 2010;29:1882-1891.
 15. Boellaard R, Delgado-Bolton R, Oyen WJG, et al. FDG PET/CT: EANM procedure guidelines for tumour imaging: version 2.0. *Eur J Nucl Med Mol Imaging*. 2015;42:328-354.
 16. Bunch PC, Hamilton JF, Sanderson GK, Simmons AH. A free response approach to the measurement and characterization of radiographic observer performance. *Appl. Opt. Instrum. Med. VI*. 1977;4:124-135.
 17. Morey AM, Kadrmas DJ. Effect of varying number of OSEM subsets on PET lesion detectability. *J Nucl Med Technol*. 2013;41:268-273.
 18. Kadrmas DJ, Oktay MB, Casey ME, Hamill JJ. Effect of scan time on oncologic lesion detection in whole-body PET. *IEEE Trans Nucl Sci*. 2012;59:1940-1947.
 19. Polycarpou I, Tsoumpas C, King AP, Marsden PK. Impact of respiratory motion correction and spatial resolution on lesion detection in PET: a simulation study based on real MR dynamic data. *Phys Med Biol*. 2014;59: 697-713.
 20. Kadrmas DJ, Casey ME, Conti M, Jakoby BW, Lois C, Townsend DW. Impact of time-of-flight on PET tumor detection. *J Nucl Med*. 2009;50:1315-1323.

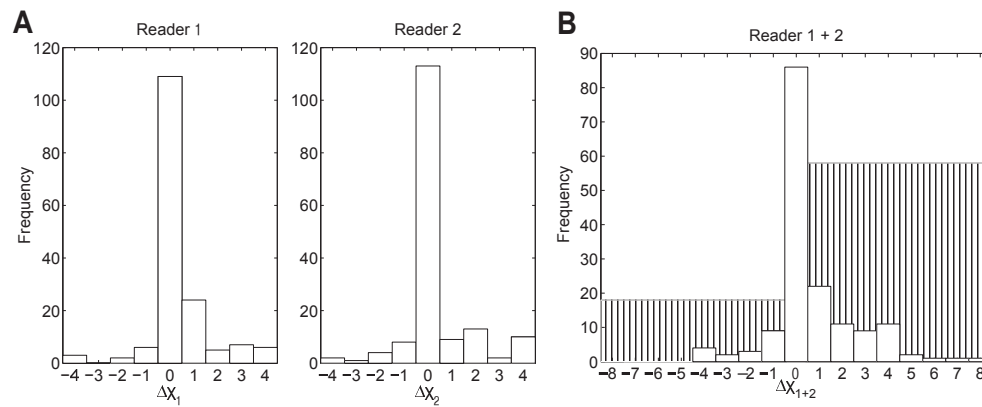


FIGURE 1: Change in confidence scores χ between uncorrected and motion-corrected images for true-positive (TP) lesions, for reader 1 only and reader 2 only (A), and for reader 1 and reader 2 score sum for each lesion (B). White bars represent the number of lesions with specific score changes. Hatched bars represent the total number of lesions with negative or positive score changes, where positive change is 'good' - TP lesions are more detectable after motion correction.

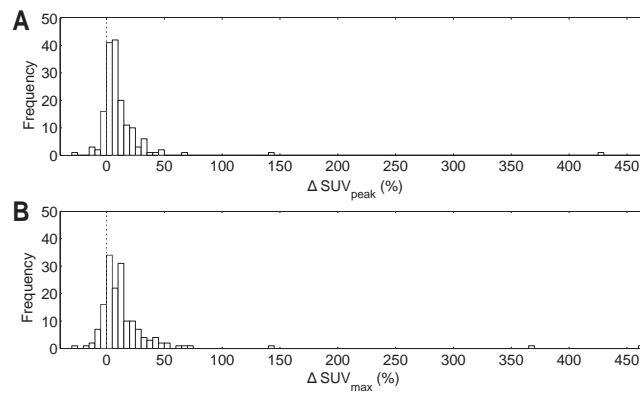


FIGURE 2: Histogram of all 162 reference lesions for metrics, $\Delta\text{SUV}_{\text{peak}}$ (A), and $\Delta\text{SUV}_{\text{max}}$ (B).

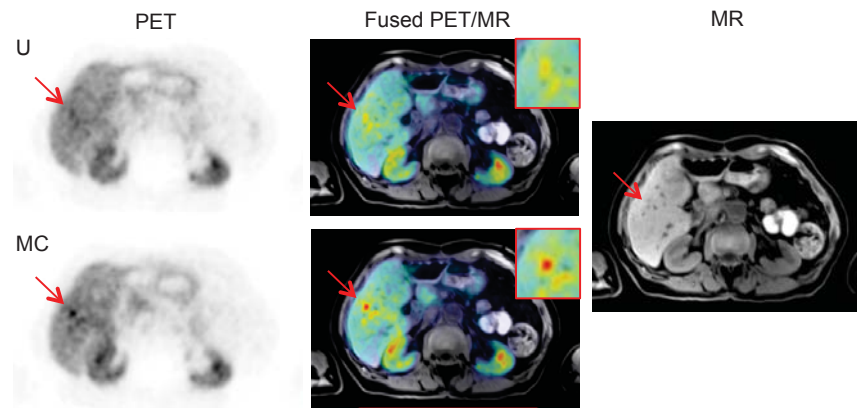


FIGURE 3: Case study 1. Lesion 1, axial slices of uncorrected (U) and motion-corrected (MC) PET images, and fused with T1 Dixon VIBE MR.

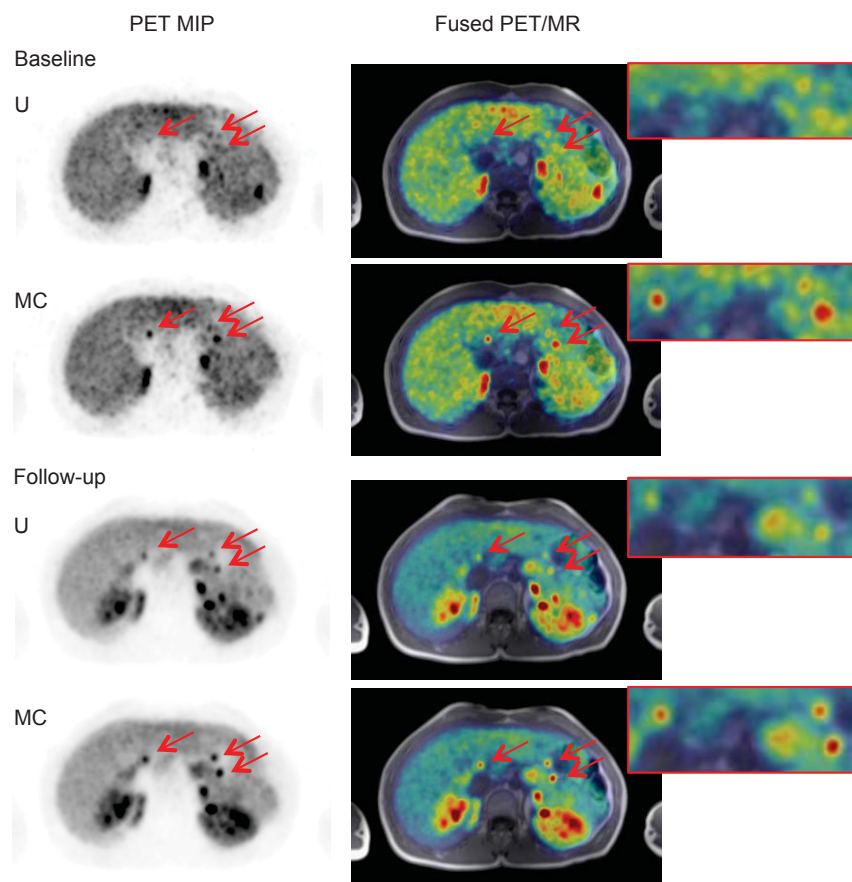


FIGURE 4: Case study 2. PET maximum intensity projection (MIP) image showing 3 pancreas lesions and axial views of uncorrected (U) and motion-corrected (MC) PET images in both the baseline and follow-up PET scans, and fused with T1 Dixon VIBE MR.

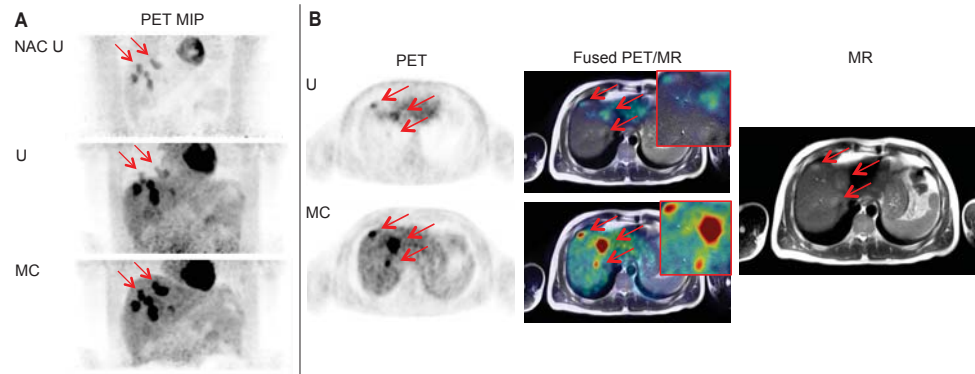


FIGURE 5: Case study 3. Maximum intensity projection (MIP) images for non-attenuation-corrected non-motion-corrected image (NAC U), attenuation-corrected non-motion-corrected image (U), and attenuation-corrected motion-corrected image (MC) (A). Axial PET slice with three lesions which wrongly appear in the lung in the uncorrected image (U) and correctly appear in the liver in the motion-corrected image (MC), and fused with T2 HASTE MR (B).

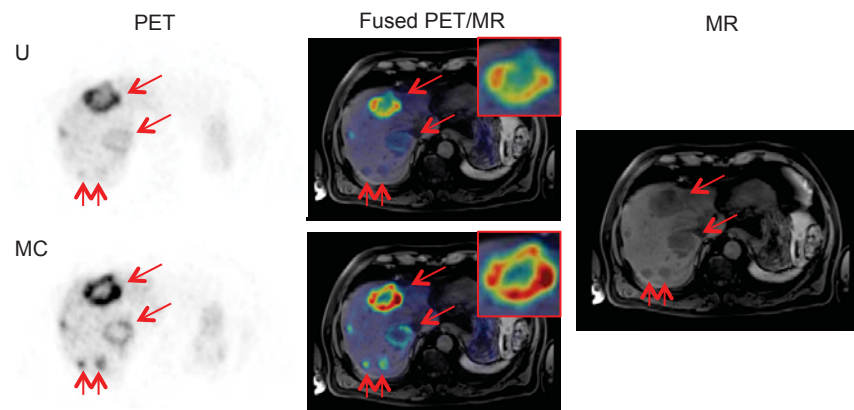


FIGURE 6: Case study 4. Coronal and axial slices of uncorrected (U) and motion-corrected (MC) PET images, and fused with T1 VIBE SPAIR MR, showing change in shape of uptake in necrotic lesion.

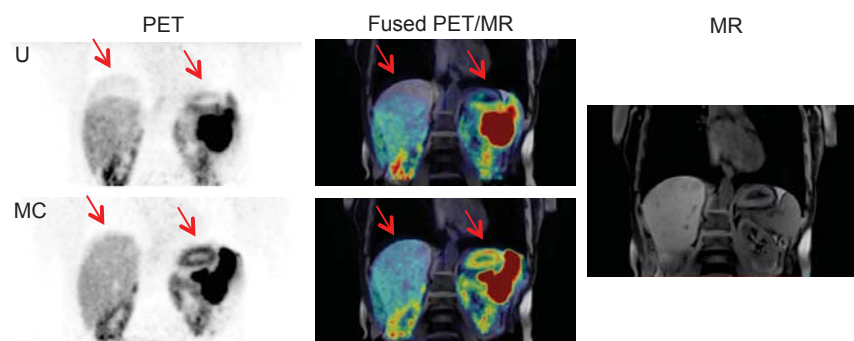


FIGURE 7: Case study 5. Coronal slice of uncorrected (U) and motion-corrected (MC) PET images, and fused with T1 VIBE MR, showing a reduction in attenuation misalignment artefacts.

PET +ve Hot Spot	Number
Liver lesion	71
Pancreas lesion	22
Lung lesion	27
Abdomen node	6
Thorax node	29
Other (kidney, bowel etc.)	7
Total	162

TABLE 1: Lesion summary in patient cohort.

All Images (42 patients, 162 lesions)			
Metric	Uncorrected	Motion-corrected	Paired Significance
SUV _{peak}	17.6±18.0	19.5±20.1	p<0.0001 (t-test)
SUV _{max}	22.7±22.6	26.6±29.9	p<0.002 (t-test)
Detection score χ	2.67 ± 1.50	3.01 ± 1.29	p<0.0001 (Wilcoxon)
TP (true-positive) rate	74%	84%	N/A
FP (false-positive)	30 lesions	21 lesions	N/A

TABLE 2: Quantitative results summary for all images. SUV metrics are means across all reference lesions. Detection scores and TP numbers are means across both readers. FP numbers are from 84 data sets (42 patients \times 2 readers). Statistical significance is based on paired scores from uncorrected and motion-corrected data sets.



The Journal of
NUCLEAR MEDICINE

Clinical Impact of Respiratory Motion Correction in Simultaneous PET/MR with a Joint PET/MR Predictive Motion Model

Richard Manber, Kris Thielemans, Brian F. Hutton, Simon Wan, Francesco Fraioli, Anna Barnes, Sebastien Ourselin, Simon Arridge and David Atkinson

J Nucl Med.

Published online: March 9, 2018.

Doi: 10.2967/jnumed.117.191460

This article and updated information are available at:
<http://jnm.snmjournals.org/content/early/2018/03/08/jnumed.117.191460>

Information about reproducing figures, tables, or other portions of this article can be found online at:
<http://jnm.snmjournals.org/site/misc/permission.xhtml>

Information about subscriptions to JNM can be found at:
<http://jnm.snmjournals.org/site/subscriptions/online.xhtml>

JNM ahead of print articles have been peer reviewed and accepted for publication in *JNM*. They have not been copyedited, nor have they appeared in a print or online issue of the journal. Once the accepted manuscripts appear in the *JNM* ahead of print area, they will be prepared for print and online publication, which includes copyediting, typesetting, proofreading, and author review. This process may lead to differences between the accepted version of the manuscript and the final, published version.

The Journal of Nuclear Medicine is published monthly.
SNMMI | Society of Nuclear Medicine and Molecular Imaging
1850 Samuel Morse Drive, Reston, VA 20190.
(Print ISSN: 0161-5505, Online ISSN: 2159-662X)

© Copyright 2018 SNMMI; all rights reserved.